JGR Oceans

RESEARCH ARTICLE
10.1029/2020JC017092

A 30 -Year Time Series of Transient Tracer-Based Estimates of Anthropogenic Carbon in the Central Labrador Sea

L. Raimondi[1], T. Tanhua[2], K. Azetsu-Scott[3], I. Yashayaev[3], and D.W.R. Wallace[1]

[1]Department of Oceanography, Dalhousie University, Halifax, Nova Scotia, Canada, [2]Division of Chemical Oceanography, GEOMAR Helmholtz Centre for Ocean Research Kiel, Kiel, Germany, [3]Department of Fisheries and Oceans, Canada, Bedford Institute of Oceanography, Dartmouth, Nova Scotia, Canada

Key Points:

- In regions of ventilation, assuming a constant tracers' saturation in the transit time distribution method results in significant negative bias of anthropogenic carbon (C_{ant}) estimates
- Annual estimates of C_{ant} column inventory between 1986 and 2016 reveal a non-steady accumulation rate of C_{ant} in Labrador Sea
- The temporal variability of the C_{ant} storage in the Central Labrador Sea appears to be linked to the strength of convection

Supporting Information:

Supporting Information may be found in the online version of this article.

Correspondence to:

L. Raimondi,
Lorenza.Raimondi@dal.ca

Citation:

Raimondi, L., Tanhua, T., Azetsu-Scott, K., Yashayaev, I., & Wallace, D. W. R. (2021). A 30-year time series of transient tracer-based estimates of anthropogenic carbon in the Central Labrador Sea. *Journal of Geophysical Research: Oceans*, *126*, e2020JC017092. https://doi.org/10.1029/2020JC017092

Received 17 DEC 2020
Accepted 5 APR 2021

Abstract We use a 30-year time series (1986–2016) of dichlorodifluoromethane (CFC-12) concentrations with a refined transit time distribution (TTD) method, to estimate the temporal variation of anthropogenic carbon (C_{ant}) in the Central Labrador Sea. We determined that the saturation of CFC-12 and sulfur hexafluroide (SF_6) in newly-formed Labrador Sea Water had departed significantly from 100% and varied systematically with time. Multiple linear regression of the time-varying saturation, with the tracer's atmospheric growth rate and the wintertime mixed layer depth as independent variables, allowed reconstruction of the saturation history of CFC-12 and SF_6 in wintertime surface waters, which was implemented in the TTD method. Use of the time-varying saturation for CFC-12 gave C_{ant} concentrations ~7 μmol kg^{-1} larger than estimates obtained assuming a constant saturation of 100%. The resulting C_{ant} column inventories were ~20% larger and displayed lower interannual variability compared to conventional TTD-based estimates. The column inventory of C_{ant} increased at an average rate of 1.8 mol m^{-2} y^{-1} over the 30-year period. However, the accumulation rate of C_{ant} was higher than this average in the early 1990s and since 2013, whereas inventories remained almost unchanged between 2003 and 2012. The variation in the C_{ant} accumulation rate is shown to be linked to temporal variability in the relative layer thickness of the annually ventilated Labrador Sea Water and the underlying Deep Intermediate Water. The non-steady C_{ant} accumulation highlights the importance of sampling frequency, especially in regions of variable deep mixing and high carbon inventories, and potential misinterpretation of C_{ant} dynamics.

Plain Language Summary Since the industrial revolution, humankind has emitted large amounts of carbon dioxide (CO_2) to the atmosphere as a result of fossil fuel combustion and cement production. About 40% of this Anthropogenic CO_2 (C_{ant}) has been sequestered by the oceans, primarily in polar and subpolar regions. The Labrador Sea has been identified as one of the regions with the highest inventory of C_{ant}. Here, as strong winds blow on the ocean's surface in wintertime, heat is lost to the atmosphere and water density increases. This process, defined as deep water convection, determines the mixing of surface water into the ocean interior and the transport of gases, like C_{ant}, from surface to depth. In this work we estimate the concentrations, column inventories and storage rate of C_{ant} in Labrador Sea between 1986 and 2016 by using gases that mimic C_{ant} behavior. We observed that despite the overall increase in C_{ant} that occurred between 1986 and 2016, the pace at which C_{ant} increased has not been constant over time in the Labrador Sea. In fact, we observed periods with both fast and slow increases of C_{ant}, which were influenced by the persistence of deep or shallow convection, respectively.

1. Introduction

The change in oceanic total dissolved inorganic carbon (DIC) concentrations relative to pre-industrial values, due to human mobilization of carbon over the past 250 years, is defined as “excess” or “anthropogenic” carbon dioxide (Excess CO_2 or C_{ant}; D. Wallace, 2001). This C_{ant} represents only a small fraction of the total dissolved CO_2, and therefore difficulties are encountered in distinguishing the anthropogenic perturbation from the predominant natural signal. This is further complicated by spatial and temporal variability of the oceanic sink for anthropogenic CO_2 (Gruber, Clement, et al., 2019; Gruber, Landschützer, & Lovenduski, 2019).

Here we take advantage of a long-time series of transient tracers (CFC-12 and SF_6) in the Central Labrador Sea, a region with high integrated column inventory of C_{ant}, to explore the temporal variability of tracer-based estimates of C_{ant} in this key region of the world's ocean for gas uptake and transport.

Methods to estimate C_{ant} in the ocean can be classified into four main categories (see Sabine & Tanhua, 2010, for a review): (1) back-calculation approaches (e.g., ΔC^*; Gruber et al., 1996) that separate observed DIC from the pre-industrial preformed DIC based on estimation of changes due to remineralization of organic matter and dissolution of calcium carbonate; (2) decadal change methods based on repeat observations (e.g., the extended multiple linear regression [MLR], eMLR; Friis et al., 2005) that identify C_{ant} by measuring differences between surveys completed in the same location but at different times; (3) model-based approaches (e.g., Ocean Circulation Inverse Model [OCIM]; DeVries, 2014) that can be used to assess the air-sea flux of C_{ant} by simulating ocean mixing, circulation, and biogeochemistry; (4) tracer-based approaches (the transit time distribution or TTD method; Waugh et al., 2006) that use transient tracers to estimate the age of a water sample and, from that, deduce its C_{ant} content based on the history of CO_2 in the atmosphere and surface water.

An important underlying assumption of most applications of these methods is that large-scale ocean circulation (e.g., ventilation of the ocean interior) is invariant over the timescale of the C_{ant} increase being considered. This steady-state assumption is particularly questionable for high-latitude regions, such as the Labrador Sea considered here, where deep water formation displays strong interannual to decadal variability (e.g., Yashayaev & Loder, 2017). Relatively few observation-based studies have addressed the validity and significance of this assumption and examined the temporal variability of C_{ant} accumulation (e.g., Carter et al., 2017; Steinfeldt et al., 2009; Tanhua & Keeling, 2012; van Heuven et al., 2011), likely because few, suitable, temporally resolved datasets are available. Similarly, modeling studies (e.g., Goodkin et al., 2011) have highlighted how errors in the ocean transport and dynamics of a model can directly affect the prediction of carbon cycle variables (e.g., air-sea CO_2 flux and C_{ant} uptake).

The Northwest Atlantic Ocean (together with the Mediterranean Sea; Schneider et al., 2010) has been shown to have amongst the highest vertically integrated concentrations of C_{ant} (DeVries, 2014; Khatiwala et al., 2009, 2013; Sabine et al., 2004; Waugh et al., 2006) in the global ocean. The Labrador Sea, in particular, is the source of Labrador Sea Water (LSW) which, together with underlying dense waters from the Denmark Strait and Iceland-Scotland Overflows, forms North Atlantic Deep Water (NADW) and therefore plays a central role for ventilating the deep ocean interior. It has previously been shown that a significant portion of the total C_{ant} that is ultimately sequestered by the North Atlantic flows through the Labrador Sea basin (Tait et al., 2000).

The formation of water masses by deep convection provides a direct path for atmospheric gases, including C_{ant}, to be exchanged with the ocean interior and has been referred to as a "trap door" mode of ventilation (Bernardello et al., 2014; De Lavergne et al., 2014). In contrast to the suppression of deep convection by a strengthening halocline in the Weddell Gyre described by Bernardello et al. (2014) and De Lavergne et al. (2014), LSW formation continues today, but is highly variable on interannual and longer timescales (Yashayaev & Loder, 2016, 2017). Further, model projections suggest there is potential for significant future reductions of convection depth and LSW formation in response to increased freshwater input from Greenland (Böning et al., 2016).

Here we present and interpret a time series of annual, tracer-based estimates of column inventories and storage rates of C_{ant} in the central Labrador Sea over a 30-year period, from 1986 to 2016. The estimates are obtained with a refined version of the TTD method applied to data collected from a long-term monitoring program conducted along the WOCE/CLIVAR/GO-SHIP repeated hydrography line AR7W. The extensive time series data available along this hydrographic transect enable us to test and/or refine two of the assumptions typically applied when using the TTD method: (a) constant (usually 100%) saturation of the transient tracers and (b) constant air-sea CO_2 disequilibrium (Matsumoto & Gruber, 2005).

Relatively few studies have focused on the spatial distribution and potential for non-steady-state behavior of C_{ant} in this region. Using the ΔC^* method (Gruber et al., 1996), Tait et al. (2000) provided the first description of the vertical distribution of C_{ant} in the Labrador Sea. This was followed by several studies which discussed the capacity of Labrador Sea to take up and store C_{ant}. For example, Terenzi et al. (2007) applied the TTD

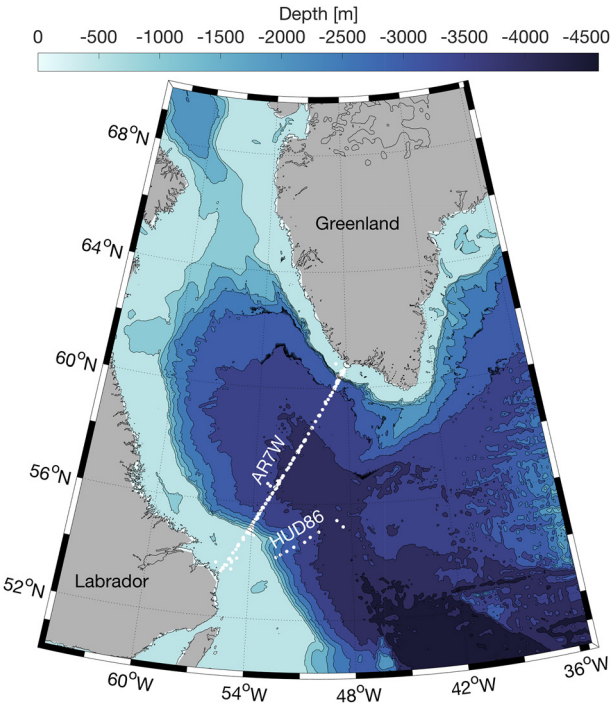

Figure 1. Map of the Labrador Sea with locations of the stations occupied during the Atlantic Zone Off-Shore Monitoring Program (AZOMP) along the AR7W section between 1992 and 2016, and during the Hudson cruise in 1986 (southernmost stations).

approach to "Classical" LSW in the North Atlantic, and suggested that, despite the high concentrations of C_{ant} in Labrador Sea, the exchange of CO_2 across the sea surface in the Labrador Sea cannot keep pace with its transport into the ocean interior. This implied that the Labrador Sea is highly undersaturated with respect to C_{ant} in the atmosphere.

Another TTD-based study by Steinfeldt et al. (2009) between 20°S and 65°N in the Atlantic identified that the maximum C_{ant} column inventory was located in the central Labrador Sea. A basin-wide decrease of the inventory within LSW was inferred between 1997 and 2003, which was explained by a temporary weakening in the rate of LSW formation and warming of the intermediate-depth waters during this period.

At the time when these studies were published it was still not possible to define whether apparent changes in column inventory were part of a long-term trend, or the result of natural (e.g., decadal) variability in water mass formation. The unusual availability of a long-time series of data from the Labrador Sea makes this area particularly valuable for identification of the nature of temporal variability in C_{ant} uptake.

2. Materials and Methods

2.1. Data

To calculate the C_{ant} with the TTD method we selected tracers and hydrographic data along a WOCE/CLIVAR/GO-SHIP repeated hydrography section (AR7W; Figure 1) that crosses the Labrador Sea, and that has been maintained by the Bedford Institute of Oceanography (BIO), Fisheries and Oceans, Canada (DFO). During these expeditions (occurring under the Atlantic Zone Off-Shore Monitoring Program [AZOMP] in recent years) samples for hydrographic, chemical, and biological parameters were collected every spring-summer along this transect (typically in May, but occasionally in June or July). For a more detailed list of the parameters measured along this section see Raimondi et al. (2019) and AR7W cruise reports at https://cchdo.ucsd.edu/.

Measurements of CFC-12 from 1992 to 2011 were subject to a secondary quality control and compiled in the GLODAPv2 data product (Olsen et al., 2016). For the years between 2012 and 2016, we performed the secondary quality control using the toolbox of Lauvset and Tanhua (2015). We also included early CFC-12 data collected in 1986 along a transect located slightly to the south of the AR7W line (Wallace & Lazier, 1988; Figure 1), which extends our data set over three decades. Sampling of SF_6 started in 2012 and annual data are available up to 2016. In Azetsu-Scott et al. (2005) and Punshon et al. (2016) a detailed description on the analytical procedures used to measure CFC-12 and SF_6 is provided.

2.2. TTD Method

We estimated the annual inventory of C_{ant} in the Central Labrador Sea between 1986 and 2016 using a refined version of the TTD method (T. Hall et al., 2002; T. M. Hall et al., 2004; Waugh et al., 2006). The TTD provides a statistical description of the age distribution of a water mass within the ocean interior (where age refers to time elapsed since a parcel of water left contact with the atmosphere within the surface mixed-layer of an isopycnal outcrop region). If water is transported into the ocean interior by advection only, a water mass could be described by a single age or "transit time," but generally mixing of water parcels with different "ages" occurs so that a water mass has a distribution or spectrum of ages. As shown by Holzer and Hall (2000), the concentration within the ocean interior of a dissolved substance subject to time-variable surface water concentrations (such as transient tracers and C_{ant}) is given by:

$$c(t,r) = \int_0^\infty c_0(t-t')G(t',r)dt' \quad (1)$$

where $c(t,r)$ is the concentration of the dissolved constituent within the ocean interior at time t and position r, $c_0(t)$ is the constituent's surface water concentration as a function of time, and $G(t',r)$ is the age distribution in the form of a Green's function that describes the propagation of surface boundary conditions into the ocean interior (Waugh et al., 2006). This distribution is commonly defined by an Inverse Gaussian function (Equation 2) characterized by a mean Γ and a width Δ.

$$G(t') = \sqrt{\frac{\Gamma^3}{4\Pi\Delta^2 t'^3}} \times exp\left(\frac{-\Gamma(t'-\Gamma)^2}{4\Delta^2 t'}\right) \quad (2)$$

The transport of water that delivers the time-variable tracer (or C_{ant}) to a certain location is characterized by the mixing of water parcels with different ages and, possibly, different source locations. The concentration of C_{ant} in the ocean interior can be estimated based on knowledge of the TTD and of the corresponding surface water concentration history of C_{ant}. The latter is obtained from the time-history of atmospheric CO_2 mixing ratios, the solubility of CO_2 and knowledge of the water mass' preformed alkalinity (TA_0; i.e., the total alkalinity [TA] of a water mass at the time it lost contact with the atmosphere). The TTD parameters, Δ and Γ, are constrained using concentrations of transient tracers such as CFC-12, CFC-11, CFC-113, CCl_4, and SF_6, and other tracers (e.g., ^{129}I; Smith et al., 2016). The ratio of width (Δ) to mean age (Γ) reflects the relative strength of diffusive to advective transport processes that connect the ocean surface to the ocean interior. Its value is generally constrained empirically by comparing mean ages obtained from different tracers with different surface water concentration histories. Purely advective transport would have a $\Delta/\Gamma = 0$ and higher ratios correspond to increasing contributions of mixing to the overall tracer transport. For the Labrador Sea, we constrained Γ and Δ using CFC-12 and SF_6 data.

Although the TTD method accounts for effects of mixing of water with different ages on tracer and C_{ant} concentrations, its use involves a number of simplifying assumptions (see Waugh et al., 2006, for a review). The first is assumption of constant saturation of surface waters (usually 100%) relative to the time-varying atmospheric concentrations of the transient tracer gases such as chlorofluorocarbons (CFCs) used to estimate the TTDs. An implication is that if the true saturation is lower than the assumed value, mean ages will be over-estimated and lower concentrations of C_{ant} will be inferred for the ocean interior. Previous studies showed that CFCs can be significantly under-saturated in newly-formed LSW (Azetsu-Scott et al., 2003; Wallace & Lazier, 1988), and dissolved oxygen also does not reach equilibrium during deep convection (Atamanchuk et al., 2020; Koelling et al., 2017).

The constant 100% saturation assumption was partially relaxed in the work of Terenzi et al. (2007), where they allowed under-saturation of the transient tracer by scaling the atmospheric history of CFC-11 to match values observed in the Labrador Sea. This scaling produced a saturation of 66%, consistent with previous observations of 60% by Wallace and Lazier (1988) and 70% by Smethie and Fine (2001), nevertheless this value was held constant in Terenzi et al.'s approach.

In the case of CFCs, under-saturation of wintertime deep mixed layer is likely to have been more pronounced during periods when the rate of increase of CFCs in the atmosphere was fastest (i.e., up to 15% $year^{-1}$ in the period between 1960s to early 1990s). Under-saturation of a tracer at the time of water mass formation is also likely to be influenced by the depth of wintertime convection (Haine & Richards, 1995). The deeper the convection, the larger the volume of water that must be equilibrated (via gas exchange) with the altered atmospheric concentration of the tracer gas. Deep convection involves entrainment of older, sub-surface water masses, typically with lower concentrations of transient tracers, which dilute tracer gas concentrations in the surface layers that are exposed to the atmosphere (Azetsu-Scott et al., 2005; Tanhua et al., 2008). Consideration of both mechanisms suggests that under-saturation of transient tracers is likely to be variable in regions of deep convection such as the Labrador Sea.

A second key assumption when applying the TTD method to C_{ant} estimation, is that the air-sea CO_2 disequilibrium has remained constant over time. Violation of this assumption might be expected given relatively long gas equilibration timescale for CO_2 (ca. 1 year) and consequent possibility that deep winter mixed-layers, that are exposed to the atmosphere for periods of weeks to months, fail to keep pace with the increase of atmospheric pCO_2 (Takahashi et al., 1997). On the other hand, the growth rate of CO_2 in the atmosphere has been steadier than that of transient tracers. Contrary to the impact of the assumption concerning tracer

gas saturation discussed above, this assumption of constant CO_2 disequilibrium may typically lead to overestimation of C_{ant} concentrations.

3. Adaptation and Application of the TTD Method to the Labrador Sea

3.1. Influence of Variable Surface Tracer Saturation to the C_{ant} Estimate

The Labrador Sea is one of the few major water-mass formation regions where historical time series of transient tracer concentrations are available with annual resolution extending over several decades. Using data from the repeated occupation of the AR7W line in May or June of each year, we reconstructed the time-varying saturation for the time of water mass formation (typically late February or March; Yashayaev, 2007; Yashayaev & Loder, 2016). We assumed that water lying between the seasonal thermocline (>200 meters [m] depth) and the maximum mixed layer depth (MLD) in the central basin best represents the water that was in contact with the atmosphere during winter. This layer is hereafter referred to as LSW. The gas saturation for each year of the time series was obtained by averaging the measured concentrations of CFC-12 and SF_6 in this LSW layer and converting these to percent-saturation based on the contemporary atmospheric mixing ratios (hereafter, the percent-saturations obtained in this way are referred to as "observed saturations").

Using a least squares method, we modeled interannual variations of the observed saturation of CFC-12 and SF_6 tracer gases at the time of convection as a function of (a) the annual rate of increase of the tracer gas's atmospheric mixing ratio and (b) the interannually-varying maximum depth of wintertime convection.

The atmospheric histories of both CFC-12 and SF_6 are well constrained. The CFC-12 atmospheric history has been reconstructed using records of production and release data from manufacturers prior to 1979 and from direct measurements after 1979 (Prinn et al., 2000; Walker et al., 2000). The SF_6 input function is based on production estimates dating back to 1953 and direct measurements since then (Bullister, 2017). The annual variation of the maximum MLD can be estimated from measurements of temperature and salinity which have been carried out in the central Labrador Sea since the 1930s (Yashayaev & Loder, 2016). The MLD was assessed through the methodology described by Yashayaev and Loder (2016) and using shipboard and Argo floats data collected by Fisheries and Oceans Canada (Yashayaev & Loder, 2017). Using the wintertime surface heat loss and the observation-based estimates of MLD, a linear regression was obtained to parameterize the MLD for years prior the early 2000s, when Argo floats data started complementing the AR7W line observations (see Section 8 of the supporting information for a detailed description of the approach). We use model MLD-4 for our calculations as this was closest to the observed MLD, and closest to the average MLD value of the four models. The regression coefficients obtained for years of observations were then used to model the saturation back to 1945 (Figure 2).

We used MLR of observed saturations to estimate the saturation of CFC-12 and SF_6 for years before the tracers were measured. The dependent variable was the observed saturation for the years 1986–2016 and 2012–2016 for CFC-12 and SF_6, respectively, and the independent variables were the first derivative of the atmospheric input function and the maximum MLD for the same years:

$$sat(LSW)(\%) = a + b \times \frac{dC}{dt} + c \times MLD \tag{3}$$

where dC/dt represents the (annual) rate of increase of the tracer's atmospheric mixing ratio and MLD is the maximum MLD in meters.

We modeled the saturation of SF_6 using both a MLR based on the 5 years of SF_6 observations, as well as using regression coefficients from the MLR obtained with the CFC-12 observations (Figure 3). The latter approach is justified because the two tracers shared quasi-exponential atmospheric histories and similar controls on air-sea exchange and uptake. We applied the regression coefficients obtained from the CFC-12 regression with the MLD time series data and the first derivative of the SF_6 atmospheric history.

Saturation variations were largely determined by the atmospheric growth rate (the root mean square error [RMSE] of the regressions using MLD alone, atmospheric growth rate alone and both atmospheric growth

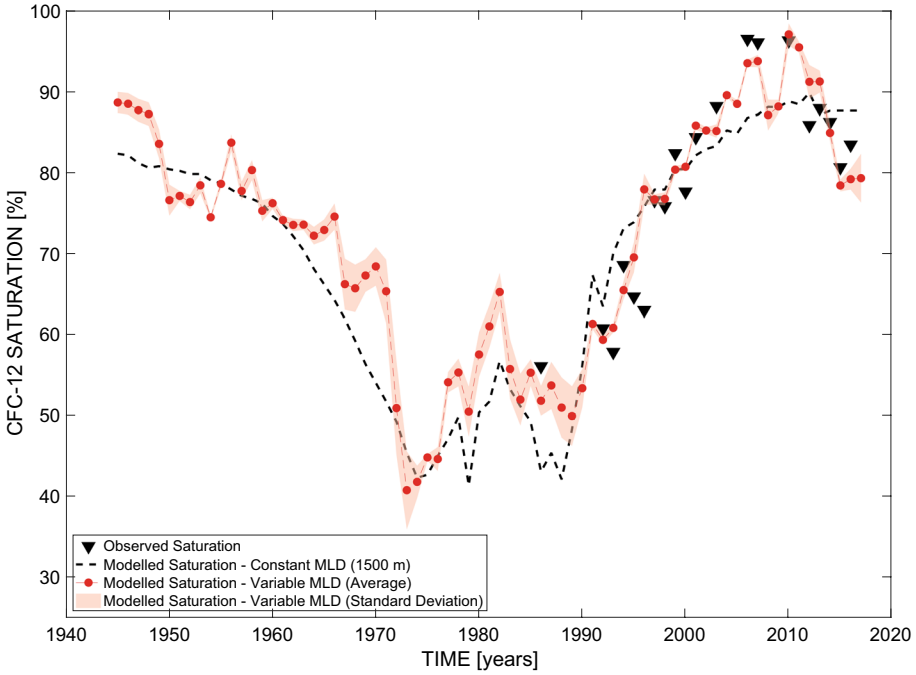

Figure 2. Modeled CFC-12 saturation during wintertime conditions in central Labrador Sea. The black triangles represent the observed saturations from 1986 to 2016. The dashed line represents the modeled saturation when the maximum MLD is assumed to be constant at 1,500 m. The dots and shaded area represent the average modeled saturation and the standard deviations obtained with a MLR involving the first derivative of the atmospheric input function and different realizations of the maximum MLD from a conceptual model (see supporting information). MLD, mixed layer depth; MLR, multiple linear regression.

rate and MLD as independent variables were 9.6%, 7.9% and 5.2%, respectively). A comparison of saturations reconstructed with a time-varying MLD (dots in Figures 2 and 3), showed that year-to-year variation of the MLD had only a small contribution of up to 17% and 12% to the overall variability of CFC-12 and SF_6 saturations, respectively. Years with saturations higher than values obtained with the constant 1,500 m MLD, indicate that the actual MLD was a shallow one (e.g., 1960–1970, 2000–2010) while lower saturations indicate years with deeper convection (e.g., 2013–2016; Figure S2).

The modeled saturations of both CFC-12 and SF_6 were then used to reconstruct the wintertime surface history of the tracer's effective mole fraction corrected for non-equilibrium conditions in central Labrador Sea using Equation 4.

$$X_{eff}(t) = \frac{(X_{atm}(t) \times sat_{LSW}(t))}{100} \tag{4}$$

where X_{eff} is the effective mole fraction (ppt) of either CFC-12 or SF_6 in air that is in equilibrium with the contemporary, wintertime surface water concentrations, X_{atm} is the tracer's atmospheric mole fraction and sat_{LSW} is the saturation calculated for newly-formed LSW in each year using the MLR (Equation 3). These calculated histories for surface water were implemented in the TTD routine so that the mean age calculation would account explicitly for the time-varying saturation of CFC-12 and SF_6. Figure 4 shows the resulting reconstructed surface histories of CFC-12 (panel a) and SF_6 (panel b) together with the atmospheric input functions of the two tracers. In Figure 4 it is noticeable that, when time-varying saturation in taken into account, both CFC-12 and SF_6 deviate significantly from the atmospheric input functions. Therefore, a large and time dependent bias is introduced when the traditional TTD approach (with assumed constant saturation of 100%) is applied to waters ventilated in the Labrador Sea.

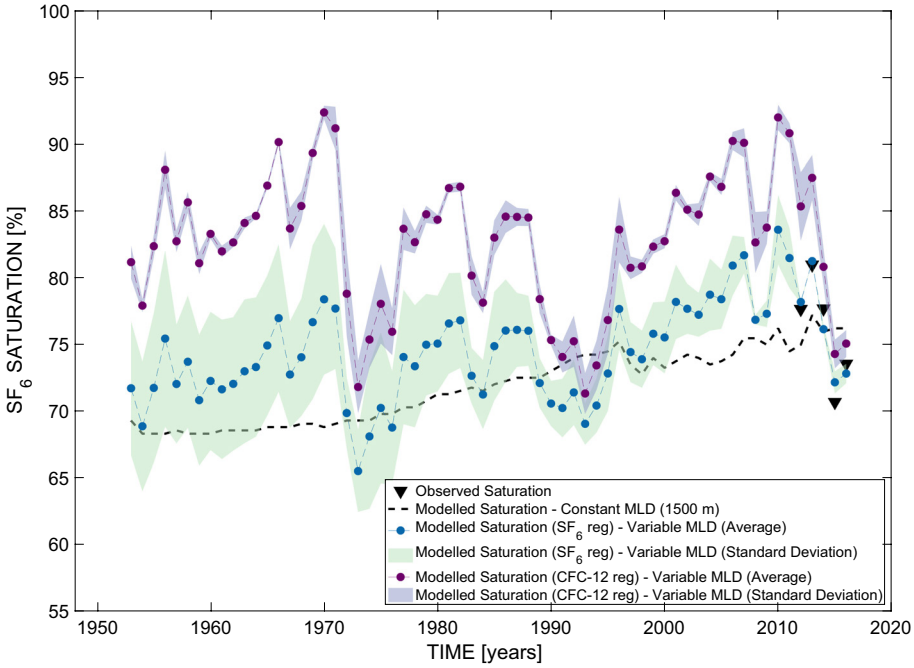

Figure 3. Modeled SF_6 saturation during wintertime in the Central Labrador Sea. The triangles represent the observed SF_6 saturations. The dashed line represents the SF_6 saturation obtained with an MLR and a constant MLD of 1,500 m. The blue dots and shading represent the average saturations and their standard deviations, respectively, obtained from the MLR performed with the SF_6 observations and the four realizations of maximum MLD. Finally, the purple dots and shading represent the average SF_6 saturations and standard deviations from the MLR performed using the regression coefficients obtained from the CFC-12 observations. MLD, mixed layer depth; MLR, multiple linear regression.

3.2. Time Variation of pCO_2

A second key assumption of the TTD approach is that the air-sea disequilibrium of CO_2 has remained constant over time. Although direct measurements of near-surface pCO_2 are not available for most of the time series, measurements of DIC and TA have been made since 1996 and allow pCO_2 to be calculated (see Raimondi et al., 2019, for description of carbonate chemistry data). For some years of the time series, TA was either not measured (from 1992 to 1995) or excluded from the GLODAPv2 data product (Olsen et al., 2016) due to lower quality of the measurements (1998–2000, 2002, 2006, and 2007). Because TA is not expected to vary systematically over time, we used a regional salinity-alkalinity relationship based on all available data to calculate TA for the years when TA measurements were not available ($TA = 41.25 \times Salinity + 862.41$; $R^2 = 0.85$).

Using the MATLAB version of the CO2SYS software (Lewis et al., 1998; Van Heuven et al., 2011), we calculated pCO_2 using the equilibrium constants from Mehrbach et al. (1973) as refit by Dickson and Millero (1987) and including measurements of salinity (S), temperature (T), pressure (P), soluble reactive phosphorus (P_T), and silicate (Si_T). From these calculated values of pCO_2 we selected only those belonging to the LSW layer and compared average values obtained for this water mass (hereafter referred to as $pCO_{2(LSW)}$) to mean values of wintertime atmospheric pCO_2 (January to April) reported from the ICE station in Iceland (Dlugokencky et al., 2019).

Figure 5 presents average values of wintertime atmospheric pCO_2 ($pCO_{2(atm)}$) and $pCO_{2(LSW)}$ over the period of measurement. Note that the calculated $pCO_{2(LSW)}$ values from (TA, DIC) agree well with independent estimates from moored sensors available in the region (red markers in Figure 5).

Although there is larger interannual variability in the oceanic pCO_2, we cannot determine whether this is representative of a time varying air-sea disequilibrium because of the uncertainty associated with the calculated pCO_2 values. The RMSE for a linear regression of $pCO_{2(LSW)}$ against time was 7.7 μatm which is smaller than the propagated random uncertainty associated with calculating pCO_2 from (TA, DIC) which

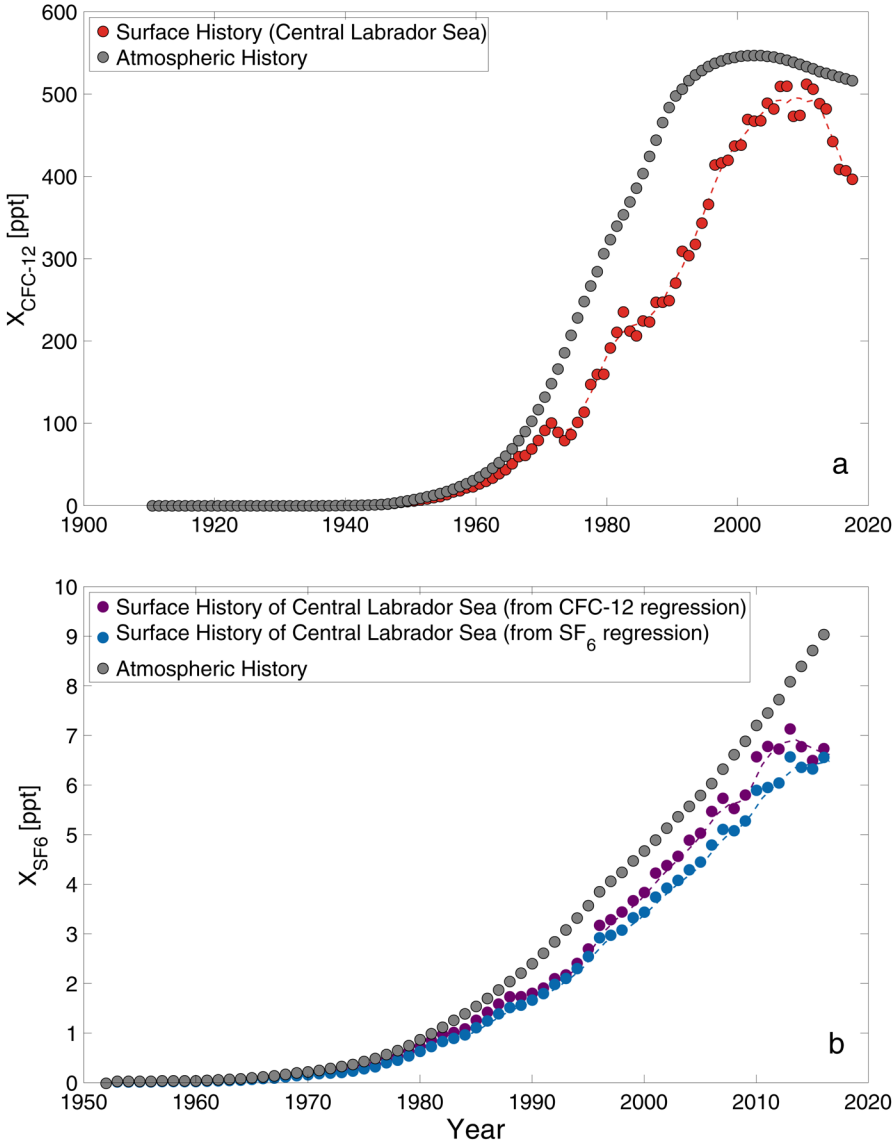

Figure 4. Panel (a) Comparison between the atmospheric history (gray dots) and the Central Labrador Sea wintertime surface history (red dots) of the X_{CFC-12} (see Equation 4). The dashed line represents the smoothed function (moving average filter) of the surface history. Panel (b) Comparison between the atmospheric history (gray dots); the Central Labrador Sea wintertime surface history of X_{SF6} obtained by applying the regression coefficients from a MLR using CFC-12 observed saturations to the SF_6 input function (purple dots) and through a MLR using observed saturations of SF_6 instead (blue dots). The dashed lines represent the smoothed functions of both surface histories of X_{SF6}. MLR, multiple linear regression.

has been estimated previously to be ~12 μatm (Raimondi et al., 2019). Hence the variability of $pCO_{2(LSW)}$ in Figure 5 is consistent with the combined random uncertainty of the dissociation constants and carbonate system measurements used in calculating pCO_2.

The rates of increase of atmospheric and LSW pCO_2 between 1996 and 2016 were 2.2 and 2.3 μatm y^{-1}. A *t*-test, performed following recommendations from Andrade and Estévez-Pérez (2014), shows that the two slopes are not significantly different from each other ($\alpha = 0.05$). We therefore conclude that $pCO_{2(LSW)}$ tracks the atmospheric increase and that there is no evidence for a time-varying air-sea disequilibrium over the period of measurement. This suggests that a constant disequilibrium assumption for pCO_2 is appropriate for use with the TTD method in this region, over this time-period.

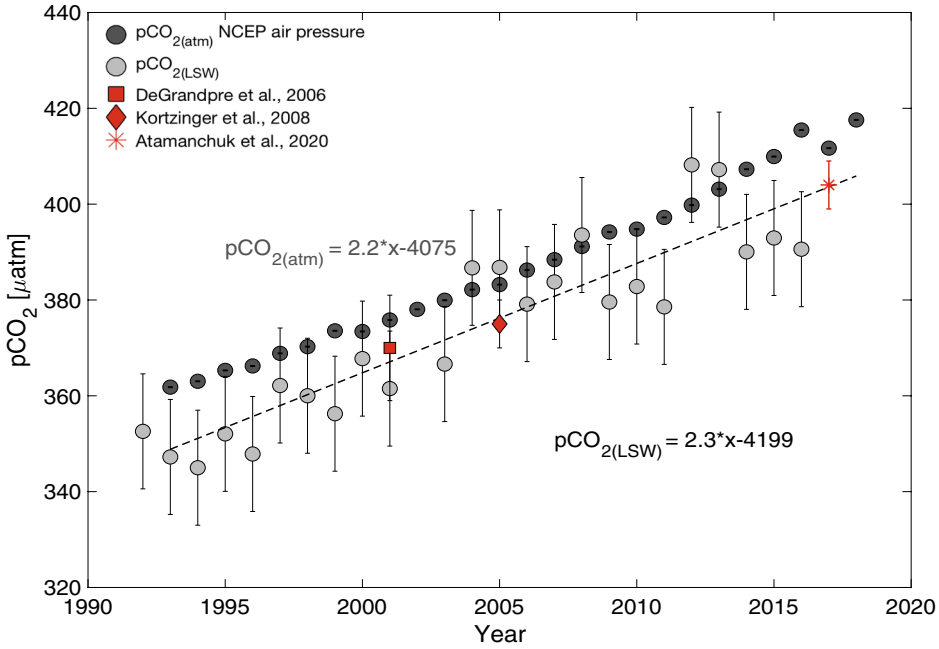

Figure 5. Average atmospheric pCO_2 and $pCO_{2(LSW)}$ values from 1992 to 2016. The atmospheric pCO_2 is a wintertime average obtained from the Iceland station data (Storhofdi, Vestmannaeyjar). The Seawater pCO_2 was calculated using (TA, DIC) as input couple in CO2SYS and averaged for the central region of Labrador Sea between seasonal thermocline and maximum MLD of each year. A S-TA relationship was obtained using our time series and then applied for those years where TA was either missing or excluded from the GLODAPv2 data. The atmospheric values of pCO_2 in μatm was obtained using NCEP values of air pressure for this region. The red square, diamond and asterisk markers represent previous estimates of pCO_2 in the region within 200 m depth by Atamanchuk et al. (2020), DeGrandpre et al. (2006), and Körtzinger et al. (2008), respectively. DIC, dissolved inorganic carbon; MLD, mixed layer depth; TA, total alkalinity.

This finding is consistent with the time evolution of the air-sea CO_2 surface disequilibrium obtained from a model simulation (Matsumoto & Gruber, 2005) which also showed little divergence between atmosphere and ocean over the years when our data were collected (~0.5 μmol C kg^{-1}, equivalent to approximately 1 μatm). It is likely that a longer time series would be required to detect any trend in air-sea CO_2 disequilibrium that is necessary to derive a larger uptake of CO_2.

3.3. Constraints on Mixing Conditions (Selection of Δ/Γ)

In contrast to some other indirect approaches of C_{ant} estimation, the TTD method accounts for water mass mixing using the Δ/Γ ratio (a measure of the breadth of the TTD). As stated by Waugh et al. (2006), two tracers with sufficiently different time histories can be used to constrain Δ and Γ. If a Δ/Γ ratio is representative of mixing conditions, the same mean age should be obtained from the different tracers. We therefore simulated mean ages based on CFC-12 and SF_6 concentrations and varied the Δ/Γ ratio between 0.4 and 2.0. We then selected the most appropriate Δ/Γ ratio based on the overall agreement of the mean ages obtained with the two tracers (Figure S1).

We performed this Δ/Γ selection by plotting the ratio of CFC-12-derived to SF_6-derived mean ages versus the SF_6-derived mean ages. Due to recently decreasing concentration of CFC-12 in the atmosphere (Figure 4a), we excluded recently formed water masses for which a consistent positive bias in CFC-12-derived mean ages was observed. We performed a linear regression using only mean ages for which SF_6 values were <6 ppt, corresponding to the time period when the CFC-12 atmospheric concentration was lower than the contemporary CFC-12 concentration. The selection was performed based on the coefficients of this regression and the average distance of the data from a reference line (black line in Figure S1 with intercept of 1 and slope of 0). The most representative ratio would be that with a slope close to 0, an intercept close to 1 and the lowest average distance of the data point from the reference line.

From this analysis, the Δ/Γ ratios that best represent the mixing conditions was 1.8.

3.4. Calculation of C_{ant} Concentrations and Inventories

The mean ages derived from this refined TTD approach were used together with the surface history of C_{ant} (obtained from atmospheric pCO_2 data and equilibrium constants) to obtain estimates of C_{ant} along the AR7W line.

Using the surface concentration histories of CFC-12 and SF_6 with variable saturation derived from the multiple linear regression, assuming constant disequilibrium for CO_2 and the Δ/Γ value selected in the previous section (Δ/Γ = 1.8), the C_{ant} concentration was calculated as:

$$C_{ant}(r,t) = \int_0^{\infty} C_{ant,0}(t-t')G(r,t')dt' \quad (5)$$

where $C_{ant,0}$ (t) is the surface concentration of C_{ant} and $G(r,t')$ is the age spectrum obtained from the tracers. The C_{ant} concentrations were then interpolated using objective mapping (Roemmich, 1983) onto a standard grid to assist with calculation of inventories for comparison between years.

In order to calculate column inventory for the central Labrador Sea (defined here as the portion of the AR7W line with bottom depth >3,300 m; Yashayaev, 2007), the gridded values of C_{ant} from the objective mapping (spatial resolution of 5 km), were averaged horizontally for 5 m depth intervals. An average C_{ant} profile was then integrated vertically to obtain a column inventory as follows:

$$I_{C_{ant}} = \int_0^{max(depth)} C_{ant,0} \times \rho \; dz \quad (6)$$

where $I_{C_{ant}}$ stands for column inventory of C_{ant}, C_{ant} is in mol kg^{-1}, ρ is the *in situ* density (kg m^{-3}). The integration was performed by using 5 m bin intervals.

In order to demonstrate the significance of the constant saturation assumption of tracers and the choice of Δ/Γ, we estimated C_{ant} using both a constant and a time-varying saturation for all Δ/Γ values listed earlier (see Results section). Finally, from the column inventories calculated for each year of the time series we calculated the storage rate (SR) in the Central Labrador Sea over three decades (in mol m^{-2} y^{-1}).

4. Results

In this section, we present results of C_{ant} concentrations obtained using the TTD method with CFC-12 data, for both a constant (100%) and a time-varying saturation (presented in Section 3.1). Results of C_{ant} obtained using the TTD method with SF_6 are provided in (Section S3.1).

4.1. Sensitivity of C_{ant} Estimates to the Saturation of CFC-12

Use of a time-varying CFC-12 saturation for TTD calculations resulted in higher estimated C_{ant}, with average differences from the conventional TTD approach of ~7 ± 1.5 μmol kg^{-1}. This translated into column inventories that were 19.2–39.7 mol m^{-2} higher when estimated with the refined TTD approach, compared to estimates based on the conventional assumption of constant (100%) saturation. In Figure 6 we show column inventories of C_{ant} calculated with both time-varying ($C_{ant(VS)}$; where the subscript VS denotes variable saturation) and constant saturations ($C_{ant(CS)}$; where CS denotes constant saturation) for Δ/Γ = 1.8.

With the constant saturation assumption, the $C_{ant(CS)}$ inventory estimates increased from 72.3 to 148.6 mol m^{-2} between 1986 and 2016, whereas the increase was from 112.0 to 181.4 mol m^{-2} when the variation of the tracer's saturation over time was accounted for. Hence, the storage rate with time-variable saturation was slightly smaller than with the traditional TTD approach (1.8 and 2.1 mol m^{-2} y^{-1}, respectively) but still within its uncertainty.

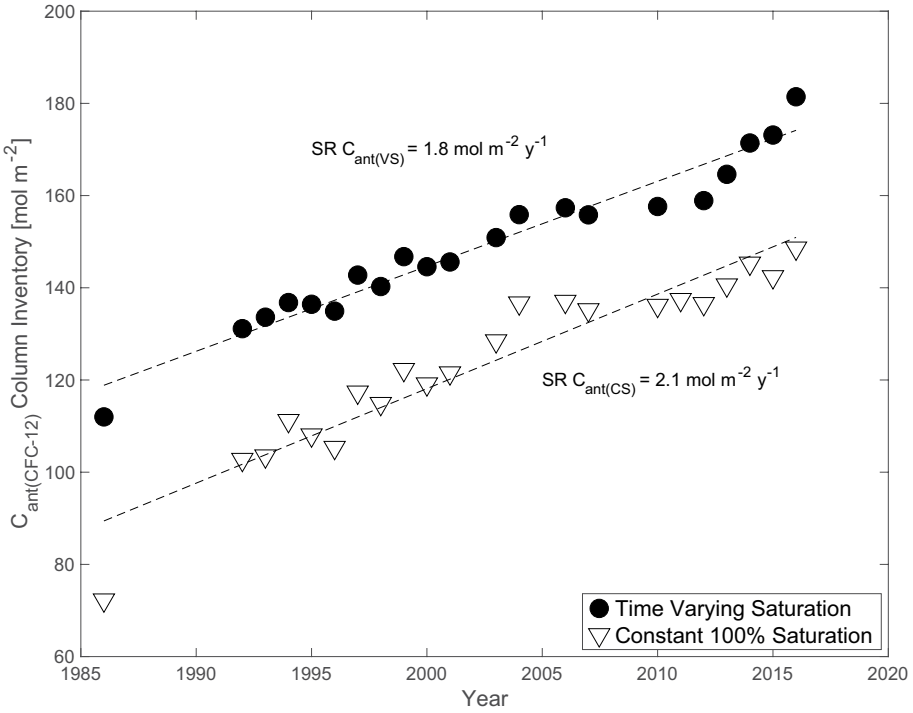

Figure 6. Column inventory of C_{ant} in the Central Labrador Sea obtained from mean ages calculated using a constant CFC-12 saturation assumption (triangles) and the column inventory obtained from our refined TTD method with $\Delta/\Gamma = 1.8$ (black dots). Here CS and VS stand for constant and variable saturation, respectively. We also report the slope of the regressions which represent the SR (in mol m^{-2} y^{-1}). SR, storage rate; TTD, transit time distribution.

Use of a time-varying saturation also reduced the interannual variability (or scatter) around the long-term rate of increase, as given by the regression line (RMSE of 5.7 and 3.7 mol m^{-2} y^{-1} using constant and time-varying saturations, respectively). The column inventory for the first year of the time-series, 1986, falls noticeably closer to the regression line when calculated with a time-varying saturation. Both approaches indicate a slow-down in the rate of increase in the early 2000s, but only the $C_{ant(VS)}$ results indicate a rapid increase in the latest years of the time series (Figure 6); a result which is also obtained using SF_6 (see Section S3.1). In fact we found that when accounting for time-varying saturation, the C_{ant} estimates based on CFC-12 agree better with those based on SF_6 (Figure S3), which is a more reliable tracer for recent years compared to CFC-12 due to decreasing atmospheric concentrations of the latter.

4.2. Sensitivity of C_{ant} Estimates to the Selection of Δ/Γ

Figure 7 presents C_{ant} column inventories for the Central Labrador Sea from 1986 to 2016 (black dots) that are averages of values calculated with the refined TTD method with CFC-12 data and using the full range of Δ/Γ ratios discussed in Section 3.3. The average column inventories increased from 114 to 182 mol m^{-2} over 30 years. The standard deviation of the inventories obtained with this range of Δ/Γ is represented by the shaded area in Figure 7 and varies between 0.6 and 2.5 mol m^{-2} in different years. This suggests that the choice of Δ/Γ does not dramatically affect the column inventory estimates. Indeed, the choice of Δ/Γ can lead to percent differences between a minimum of −4.5% and a maximum of 0.4% in C_{ant} concentrations compared to the reference concentrations obtained with $\Delta/\Gamma = 1.8$ (Table S1). This translated into a maximum difference of ∼1.2% in column inventory estimates using different ratios. We note that Hsieh (2016) suggested that the Δ/Γ ratio should be variable over time to better represent the different mixing conditions at times of intense and weak convection. However, our results show that the choice of Δ/Γ will not dramatically affect our estimates of C_{ant} column inventories and therefore, for this study, the Δ/Γ ratio was held constant over time.

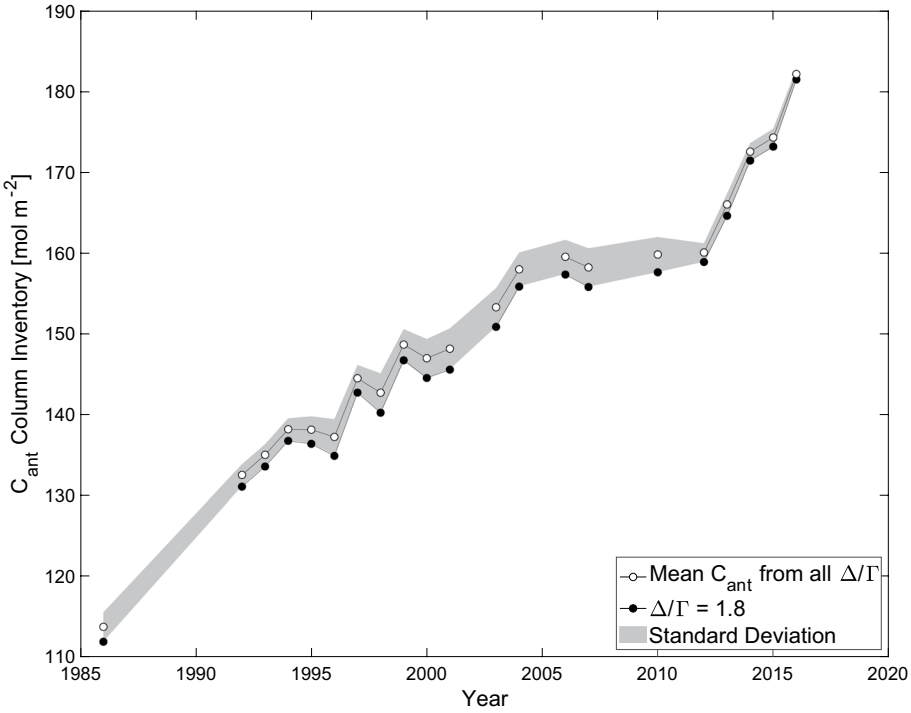

Figure 7. Average column inventories of C_{ant} in the Central Labrador Sea from 1986 to 2016 obtained from CFC-12 (white dots). These averages were calculated using C_{ant} estimates obtained from a wide range of Δ/Γ (0.4–2.0) and time variable saturation. The shaded area represents the standard deviation obtained for the range of Δ/Γ. For reference, we also report the column inventories obtained with the selected Δ/Γ of 1.8 (black dots).

4.3. Distribution of C_{ant} in Major Water Masses

Below the seasonal thermocline (i.e., >200 m depth) the vertical structure of the Central Labrador Sea is dominated by a homogeneous cold and fresh layer defined as LSW. Depending on the depth of convection reached every year, the lower limit of the LSW layer can be usually found between 500 and 2,000 m depth, with the deepest convection ever observed reaching as deep as 2,400 m in 1993 and 1994 (Yashayaev, 2007; Yashayaev & Loder, 2016). Below the LSW lies the more saline North East Atlantic Deep Water (NEADW) which originates from the Iceland-Scotland Overflow Water that enters the North Atlantic through the Iceland-Faroe-Scotland Ridge and becomes more saline due to mixing with overlying salty and warm Atlantic Waters (thermocline water in the lower limb of the Subpolar Mode Water and North Atlantic Current) that add characteristic salt to the mix (Yashayaev & Dickson, 2008). Below the NEADW layer, lies the cold, dense and less saline Denmark Strait Overflow Water (DSOW). This is the densest water mass observed in the Labrador Sea and the entire Subpolar North Atlantic (SPNA). It originates from the Denmark Strait Overflow and enters the basin from the Greenland Sea via the Irminger Sea (Yashayaev, 2007).

We identified these water masses based on either their time-varying or fixed density ranges (σ_2; for LSW and NEADW, respectively) or depth range (for surface water and DSOW), and calculated both the average C_{ant} concentrations and the individual contributions to the total column inventory of these water masses (see Tables S2 and S3 for water masses definitions, some of which have varied over time). As a further step we identified the contribution to the total C_{ant} column inventory of a body of water here referred to as Deep Intermediate Water (DIW). This water mass is a mixture of LSW, NEADW, Icelandic Slope Water (Yashayaev & Loder, 2017) and other intermediate and deep-water masses of the SPNA. The DIW is the product of modification and transformation of a deep-reaching and dense class of LSW formed between 1987 and 1994, possibly with smaller, occasional additions of dense water formed in subsequent years. The aging of this old class of LSW ($LSW_{1987–1994}$ in Yashayaev, 2007) is reflected in the steady loss of its original high freshwater and oxygen signatures, which eventually determined DIW to be almost indistinguishable from

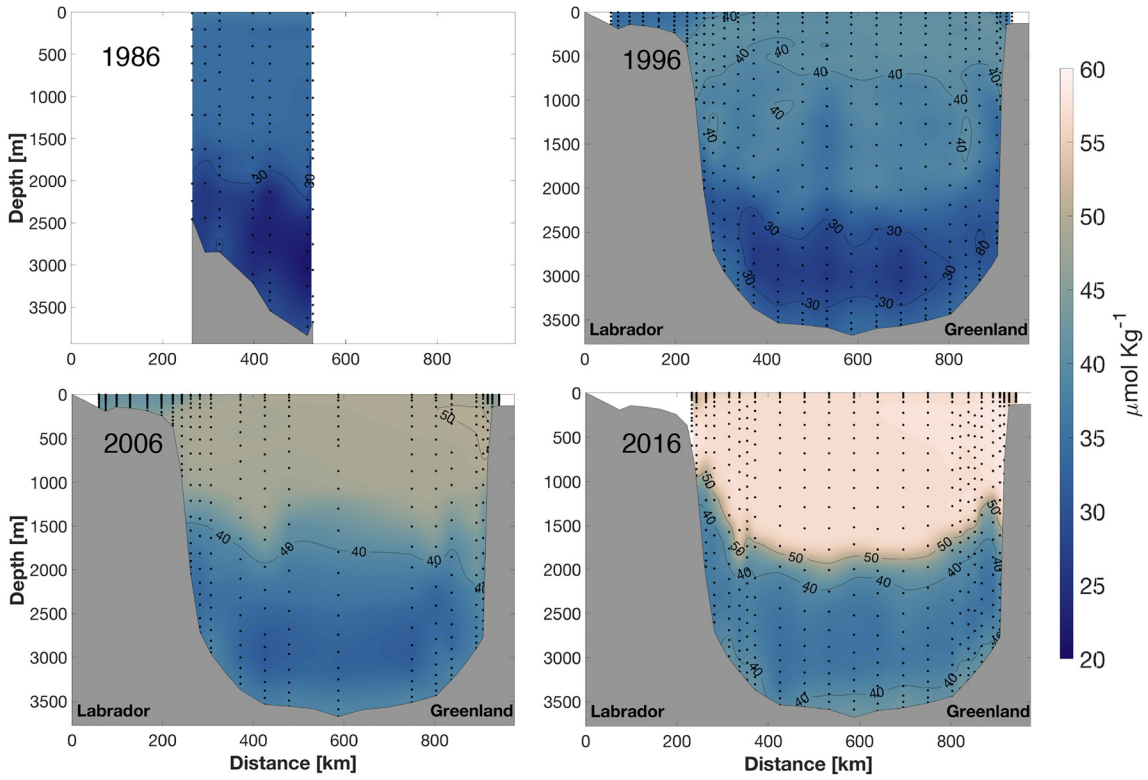

Figure 8. Sections of C_{ant} along the AR7W line (except for data in 1986 which were collected further south) obtained from the refined TTD method. The sections show the strong increase and deep entrainment of C_{ant} in Labrador Sea. TTD, transit time distribution.

NEADW. Similarly to new LSW formation, the DIW shows strong temporal variability of its layer thickness (Figure 9d).

In Figure 8, we present selected C_{ant} sections from 1986, 1996, 2006, and 2016 to illustrate the multi-decadal increase and deep penetration of C_{ant} throughout the Labrador Sea (for the full time series we refer to the animation provided as supplementary material). The sections, are similar to the vertical distribution of C_{ant} described by Tait et al. (2000). The highest concentrations of C_{ant} are found, by definition, in the surface layer (<200 m) which is underlain by a relatively homogeneous layer of high concentrations extending down to 1,500–2,000 m (this is the layer of water that is primarily ventilated in Labrador Sea). The depth range of the older NEADW (2,400–3,400 m) is marked by a minimum in C_{ant} concentrations, whereas an increase in concentrations within 200 m above the seabed reflects the presence of more recently ventilated DSOW.

5. Discussion

5.1. Interannual Variability of C_{ant} in Major Water Masses

In Figure 9a, we present the temporal variation of the average and standard deviation of the C_{ant} concentrations in the major water masses discussed in the previous section. Between 1986 and 2016, the average C_{ant} concentration of LSW increased by 22 μmol kg^{-1}, whereas notably smaller increases were observed in the other water masses (13 μmol kg^{-1} in both DIW and NEADW; 12 μmol kg^{-1} in DSOW). This implies that the rate of increase of the annual mean C_{ant} concentrations is the fastest in LSW (at 0.8 μmol kg^{-1} y^{-1}), showing that this is the water mass that primarily drives the overall variability of C_{ant} around the long-term (multi-decades) trend observed in the region. The DIW showed an overall temporal increase similar to that of NEADW and DSOW, but also showed higher interannual variability in C_{ant} concentrations as with LSW (Figure 9a).

As noted earlier, the DIW is primarily composed of LSW left over from previous years of strong convection, and not just $LSW_{1987–1994}$, and was therefore originally characterized by high concentrations of C_{ant}.

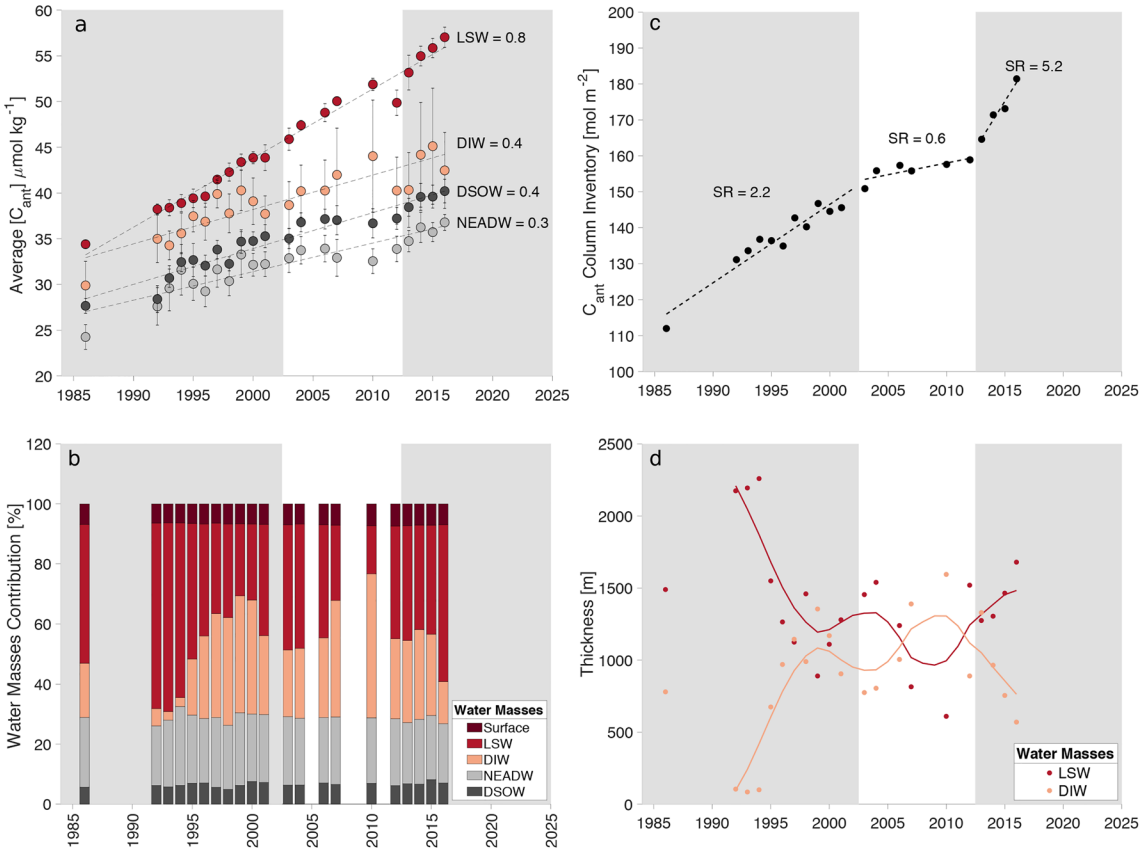

Figure 9. Panel (a) Average C_{ant} concentrations and standard deviations in LSW, DIW, NEADW, and DSOW in the Central Labrador Sea between 1986 and 2016. Next to each water mass we report the rate of increase of the average concentration in μmol kg^{-1} y^{-1} (i.e., slopes of the regressions). Panel (b) Breakdown of the percent contribution of different water masses to the C_{ant} column inventory in the Central Labrador Sea. Panel (c) Time evolution of C_{ant} column inventories from 1986 to 2016 with regressions for three periods. Note that SR represents the slope of each of the three regressions (in mol m^{-2} y^{-1}). Panel (d) Time evolution of the LSW and DIW layer thickness between 1986 and 2016, dots represent absolute values, solid line represent smoothed 5 years running means. DIW, Deep Intermediate Water; DSOW, Denmark Strait Overflow Water; NEADW, North East Atlantic Deep Water; SR, Storage Rate.

Nevertheless, while LSW is ventilated from the surface every year and therefore exposed to increasing C_{ant} concentrations, the DIW becomes progressively older, explaining why its rate of increases of C_{ant} is similar to that of NEADW.

Both the annual mean concentrations and rate of increase of C_{ant} are higher in DSOW than in NEADW (Figure 9a). This is explained by the more recent ventilation of the former and by the stronger transformation and modification the NEADW undergoes when arriving into the Labrador Sea (Yashayaev & Dickson, 2008). Further a smaller fraction of annual addition of the original overflow water mixes into NEADW compared to DSOW.

In Figure 9b we present the percentage contributions of the four main water masses, as well as the surface water, to the C_{ant} column inventory of the Central Labrador Sea over time. The figure shows that NEADW and DSOW, which are ventilated outside the Labrador Sea, display a stable contribution to the total inventory. On the other hand, LSW and DIW, which both are ventilated, at least partially, in the Labrador Sea, show large variability in their relative contributions. Whereas LSW's contribution dominated the column inventory in the early 1990s and in the most recent years, DIW contributed significantly during the intervening years, reflecting the decreased LSW layer thickness. The LSW and DIW exhibited stronger interannual variability of their contribution to the C_{ant} column inventory due to changes in their relative layer thickness (Figure 9d), this is reflected by wider ranges of percent contribution for LSW and DIW (between 16%–63% for LSW; 3%–48% for DIW) compared to narrower ranges for NEADW and DSOW (20%–26% for NEADW and 5%–8% for DSOW).

5.2. Non-Steady Accumulation of C_{ant} in the Central Labrador Sea

The time series of C_{ant} column inventory (Figure 6) shows that the increase in column inventory is not steady over time. In particular we observed three distinct periods: 1986–2002, 2003–2012, and 2013–2016 (Figure 9c). We find that whereas the first and third periods were characterized by intermediate and fast increase of C_{ant} column inventory respectively (2.2 and 5.2 mol m^{-2} y^{-1}), the period between 2003 and 2012 was characterized by a low accumulation rate (0.6 mol m^{-2} y^{-1}). This accumulation rate was not significantly different than zero therefore indicating that the C_{ant} column inventory remained constant at this time.

During the first period (between 1986 and 2001) the average C_{ant} concentrations of LSW and DIW displayed differences <5 μmol kg^{-1} (Figure 9a). During this time, the Labrador Sea experienced both deep (1992–1995) and intermediate (1996–2002) convection, which was responsible for a shift from a LSW-dominated water column to one that was equally partitioned between LSW and DIW (Figure 9d). During this first period, the average concentrations of C_{ant} were the lowest throughout the time series and not very different in these two water masses, therefore the relative proportion of the two water masses did not matter to the extent it did in later years of the time series. Further, whereas the rate of increase of C_{ant} average concentrations in DIW at this time (0.6 μmol kg^{-1} y^{-1} between 1986 and 2002) was the same as that observed toward the end of the time series (0.7 μmol kg^{-1} y^{-1} between 2013 and 2016), the rate of increase in the LSW during this first period (0.7 μmol kg^{-1} y^{-1} between 1986 and 2002) was considerably lower than what was observed toward the end of the time series (1.3 μmol kg^{-1} y^{-1} between 2013 and 2016). As a result, we observed only an intermediate storage rate of C_{ant} despite this being the period when the deepest convection was observed.

Starting in 2003, and continuing for the remainder of the time series, we observed a divergence of the LSW and DIW C_{ant} concentrations, with LSW displaying progressively higher average concentrations than DIW (Figure 9a). During this second period of our time series (between 2003 and 2012), the formation of LSW became progressively shallower and the DIW became the main water mass contributing to the total inventory of C_{ant}. The combination of lower formation of LSW, consequent predominance of DIW (Figure 9d), the much lower concentrations of C_{ant} displayed in DIW compared to LSW and the lowest rate of increase of C_{ant} in both water masses (0.5 and 0.3 μmol kg^{-1} y^{-1}, for LSW and DIW, respectively), resulted in the low accumulation observed between 2003 and 2012 (Figure 9c).

During the third period (between 2013 and 2016), there was renewed formation of LSW, and this time the water mass displayed large average concentrations of C_{ant} (which were larger than the concentrations observed in the DIW layer) and the highest rate of increase observed (1.3 μmol kg^{-1} y^{-1}). The increase in the thickness of the LSW layer coupled with its high C_{ant} concentrations, resulted in the fastest accumulation rate of C_{ant} observed over the 30-year time series (Figure 9a).

Therefore, we find that the combination of variability in the relative layer thickness of LSW and DIW and their average C_{ant} concentrations leads to significant multi-year variability in the rate at which C_{ant} is stored in the Labrador Sea.

This is consistent, overall, with the findings of Steinfeldt et al. (2009), that C_{ant} accumulation in LSW is not steady over time. Nevertheless, whereas they detected a slow-down of C_{ant} accumulation in LSW throughout the northwest Atlantic between 1997 and 2003, our study demonstrates a period of slow-down in C_{ant} accumulation within the Central Labrador Sea (the formation region for LSW) that starts in 2003 and continued until 2012.

There are several potential reasons for this apparent discrepancy between our findings and those of Steinfeldt et al. (2009). For example, the lower-than-expected accumulation between 1997 and 2003 in the Steinfeldt et al.'s study might have been caused by their assumption of constant saturation of transient tracers when estimating C_{ant}. Alternatively, the very significant differences in the temporal and, especially, spatial distribution of the data used in the two studies complicates any comparison of the two estimates. Our study has high temporal resolution, but is confined to the immediate formation region of LSW, whereas Steinfeldt et al. (2009) compare only two "snapshots" of C_{ant} distributions, but those snapshots involve LSW that is distributed throughout the Sub-Polar Gyre of the North Atlantic.

Our saturation reconstruction (Figures 2 and 3) shows that the period between 1997 and 2003 addressed by Steinfeldt et al. (2009) was characterized by strong under-saturation of both CFC-12 and SF_6, implying

that CFC-11, which was used to estimate C_{ant} in 1997 in their work, was likely also undersaturated. While the possibility of under-saturation was taken into account by Steinfeldt et al. (2009), using values between 65% and 100% depending on the density layer, the saturation values were held constant over time. Applying a constant 65% saturation to the calculation of C_{ant} inventories along the AR7W line, increases our estimates by 12% for 1997 and 18% for 2003, compared to estimates based on an assumed constant saturation of 100%, bringing our estimates closer to those reported in Steinfeldt et al. (2009). Nevertheless, our C_{ant} column inventory estimates for the central Labrador Sea in 1997 are significantly lower (~10–40 mol m^{-2}) than those reported in Figure 5 of Steinfeldt et al. (2009), irrespective of whether we use a time-varying or a constant 65% saturation. For this reason, we do not see a slow-down in C_{ant} accumulation until later in the time series.

It is important to emphasize that the slow-down in C_{ant} storage rate was only temporary (ca. 10 years) and not representative of the overall trend throughout the three decades. In particular we observed a recovered fast storage rate in the latest years of the $C_{ant(VS)}$ time series (note that this would not have been observed if a constant 100% saturation had been assumed) which corresponds with renewed deep winter convection during this period (Yashayaev & Loder, 2016).

Rhein et al. (2017) reported C_{ant} estimates based on the TTD method for Central Labrador Sea between 1992 and 2016, however in contrast to this study they only considered constant saturation of CFC-12. Further, Rhein et al. (2017) assessed the C_{ant} inventory in two adjacent density layers: the upper LSW (uLSW) and deep LSW (dLSW) as defined in Stramma et al. (2004), however this partitioning of the upper-to-intermediate water column into two density layers does not necessarily reflect the time evolution of newly-formed LSW and the associated LSW classes (Yashayaev, 2007; Yashayaev & Loder, 2016, 2017). Our approach was to define water masses as water with homogeneous property distributions, with LSW defined following Yashayaev (2007), and later revisited in Yashayaev and Loder (2016, 2017), and NEADW and DSOW defined as in Yashayaev and Dickson (2008). For comparison purposes in Figures S3 and S4, we have also reported results using the uLSW and dLSW layer definitions.

Overall, our C_{ant} estimates are comparable to those reported in Figure 3b of Rhein et al. (2017), even though some discrepancies are to be expected due to the use of the refined TTD method in our study. The slow-down in Cant storage rate that we observed between 2003 and 2012 appears to be consistent with findings in Rhein et al. (2017). These authors report that the C_{ant} inventory in the LSW layer (uLSW + dLSW) in 2007–2010 was lower than the value projected based on data from 1996 to 1999 and assuming no changes in ventilation had occurred. This difference was attributed to a decrease in ventilation rate and supported by a decrease in the fraction of LSW younger than 20 years (see Figure 5 in Rhein et al., 2017). We show that the decreasing thickness of LSW between 2003 and 2012, and increased thickness of DIW due to transformation of old LSW into DIW (which is characterized by low C_{ant} concentrations), not only affects the C_{ant} inventory of the LSW but also the overall accumulation of C_{ant} in the Central Labrador Sea, as demonstrated by the lack of column inventory increase during this second period of the time-series.

Using the same GLODAPv2 data product Gruber et al. (2019) provided global estimates of decadal changes in C_{ant} between the JGOFS/WOCE era (1982–1999) and the GO-SHIP era (2000–2013) based on their eMLR (C*) approach. From this study, it emerged that the Labrador Sea has experienced an increase of ~15 mol m^{-2} over the period 1994–2007, which corresponds to a storage rate of 1.15 mol m^{-2} y^{-1}. Our C_{ant} estimates showed an increase of 19 mol m^{-2} in column inventory based on the difference between these two years which, when divided by the number of years elapsed results in a storage rate of 1.46 mol m^{-2} y^{-1}. On the other hand, if we use the annual estimates and calculate the storage rate as the slope of a linear regression for this time period we find a storage rate of 1.8 mol m^{-2} y^{-1} instead. Both of these approaches assume a steady linear increase in C_{ant} column inventories, which we have shown is unlikely in Labrador Sea where the storage rate can change significantly over short periods of time.

The differences between these accumulation rates can potentially be related to the different methodologies applied to estimate C_{ant} and the different time resolution of the two studies. Whereas we used a tracer-based approach (the TTD method), Gruber et al. (2019) used the eMLR(C*) method which is based on DIC measurements as well as other oceanographic variables (i.e., temperature, salinity, nutrients, etc.). As mentioned

previously we know that while on a global scale these methods can produce estimates that agree within their uncertainties, disagreements can occur on a regional scale (Khatiwala et al., 2013).

Further, the discrepancies between accumulation rate estimates highlights the importance of sampling frequency and the assumption of steady linear increase of C_{ant}, especially in highly variable regions like the Labrador Sea. While for most of the world oceans sampling at a decadal frequency allows to track the uptake and inventory of C_{ant} (Sloyan et al., 2019), we show here that this is most likely not the case for the Labrador Sea. Depending on the years analyzed, conclusions on the accumulation of C_{ant} in Labrador Sea could be significantly biased depending on the temporal sampling resolution.

6. Conclusions

In this study we calculated annual estimates of column inventory and the multi-decadal, average storage rate of C_{ant} in the Labrador Sea using a refined version of the tracer-based, TTD approach from 1992 to 2016 and extended further to 1986.

We analyzed the validity of two assumptions used conventionally with the TTD approach: the transient tracers' constant saturation (often assumed to be 100%); and constant air-sea CO_2 disequilibrium.

The saturation of CFC-12 and SF_6 over time was reconstructed using a multiple linear regression approach with the rate of increase of the tracers' atmospheric mixing ratios (first derivative of the atmospheric input functions) and maximum MLD as independent variables. We found that the atmospheric input function was the most important controlling factor of the tracers' saturation. Both CFC-12 and SF_6 were under-saturated in wintertime surface waters throughout the three decades of observations in this region so that a significant bias can be introduced if the TTD method is applied assuming constant 100% saturation. Our refined TTD method, accounting for a time variable saturation of transient tracers, resulted in higher column inventory estimates (18% difference on average) and slower storage rates (17% lower storage rate) than the conventional approach (Figure 6). Accounting for time-varying saturation also led to better agreement between C_{ant} column inventories estimated through CFC-12 and SF_6 compared to when using a constant 100% saturation.

With regard to the second assumption of the TTD method, values of pCO_2 calculated from our measurements showed that, for the time-period of observations, a constant air-sea CO_2 disequilibrium is an adequate assumption in this region.

Hence, this study shows the critical importance of assumptions when using indirect, tracer-based approaches to estimate the concentration of C_{ant}. As noted previously (D. Wallace, 2001; D. W. Wallace, 1995; Waugh et al., 2006), CFCs are not an exact analog or proxy for a reactive, high-solubility gas like CO_2, so testing of assumptions and approaches can be key to inferences of C_{ant} behavior.

With this refined TTD method, we estimated an overall increase of 69 mol m^{-2} in the average column inventory in the Central Labrador Sea between 1986 and 2016 resulting in an average storage rate of 1.8 mol m^{-2} y^{-1} (roughly three times the global average accumulation rate estimated by Gruber et al., 2019). However, the accumulation rate was not steady over time. A slowdown in the accumulation of C_{ant} was observed between 2003 and 2012 in the Central Labrador Sea (SR = 0.6 mol m^{-2} y^{-1}). Nevertheless, the slowdown was temporary, and an increase in column inventories was re-established between 2013 and 2016 at a faster pace (SR = 5.2 mol m^{-2} y^{-1}) compared to that observed in the 1990s (SR = 2.2 mol m^{-2} y^{-1}).

These variations in the accumulation rate of C_{ant} were associated with changes in the annual depth of convection, and therefore with differences in the mean C_{ant} concentrations in LSW and DIW. In particular, 2003–2012 slow-down in C_{ant} accumulation was associated with shallower LSW formation and a predominance of DIW with lower mean C_{ant} concentrations than LSW, at that time.

The non-steady accumulation of C_{ant} in the Labrador Sea highlights the importance of sampling frequency in highly variable regions like the Labrador Sea. In fact while decadal repeated occupations of oceanographic sections allow the overall increase of the C_{ant} column inventory to be observed (Gruber et al., 2019; Sabine et al., 2004), important interannual and sub-decadal variability can be missed with this sampling frequency. The arbitrary selection of sampling years could lead to misinterpretation of C_{ant} dynamics in regions like the

Labrador Sea, for example when the two years sampled happened to be extremely divergent from the overall, long-term trend. Further with this study we have shown the importance of long-time series in testing assumptions of methodologies used to estimate C_{ant}.

Accounting for the whole Labrador Sea (here defined as the region between 52–66°N and 42–65°W), using a gridded bathymetry and assuming that the C_{ant} concentrations measured along the AR7W line are spatially uniform throughout, we estimated the total inventory of C_{ant} stored in this region. This inventory has increased from 0.9 to 1.5 Pg C between 1986 and 2016, meaning that the Labrador Sea, despite representing only 0.1% of the world's ocean volume, stores ~1% of the global inventory of C_{ant} (compared to the "best-estimate" inventory of 155 Pg C reported by Khatiwala et al., 2013). This estimated total inventory of C_{ant} for the Labrador Sea is equivalent to ~11% of Canada's total CO_2 emissions between 1992 and 2016 (Environment & Climate Change Canada, 2020).

Data Availability Statement

Data from the GLODAPv2 data product can be found at https://www.glodap.info/.

Acknowledgments
This work was supported by the Canada Excellence Research Chair in Ocean Science and Technology (CERC.OCEAN), the Ocean Frontier Institute (OFI), the NSERC CREATE Transatlantic Ocean System Science and Technology (TOSST) program, the Ventilation, Interaction and Transports Across the Labrador Sea (VITALS) program and the Department of Fisheries and Ocean's Atlantic Zone Off-Shore Monitoring program (AZOMP). The author would like to acknowledge the efforts by the Chief Scientists, Captains, and crew members of the *C.C.G.S. Hudson* who provided fundamental support throughout the years to maintain this invaluable time series along AR7W. Finally, the author would like to thank Stephen Punshon for his meticulousness in measuring CFC-12 and SF_6 and for the helpful insights on transient tracers.

References

Andrade, J. M., & Estévez-Pérez, M. G. (2014). Statistical comparison of the slopes of two regression lines: A tutorial. *Analytica Chimica Acta*, *838*, 1–12. https://doi.org/10.1016/j.aca.2014.04.057

Atamanchuk, D., Koelling, J., Send, U., & Wallace, D. W. R. (2020). Rapid transfer of oxygen to the deep ocean mediated by bubbles. *Nature Geoscience*, *13*(3), 232–237. https://doi.org/10.1038/s41561-020-0532-2

Azetsu-Scott, K., Jones, E. P., & Gershey, R. M. (2005). Distribution and ventilation of water masses in the Labrador Sea inferred from CFCs and carbon tetrachloride. *Marine Chemistry*, *94*(1–4), 55–66. https://doi.org/10.1016/j.marchem.2004.07.015

Azetsu-Scott, K., Jones, E. P., Yashayaev, I., & Gershey, R. M. (2003). Time series study of CFC concentrations in the Labrador Sea during deep and shallow convection regimes (1991–2000). *Journal of Geophysical Research*, *108*(C11). https://doi.org/10.1029/2002jc001317

Bernardello, R., Marinov, I., Palter, J. B., Galbraith, E. D., & Sarmiento, J. L. (2014). Impact of Weddell Sea deep convection on natural and anthropogenic carbon in a climate model. *Geophysical Research Letters*, *41*(20), 7262–7269. https://doi.org/10.1002/2014gl061313

Böning, C. W., Behrens, E., Biastoch, A., Getzlaff, K., & Bamber, J. L. (2016). Emerging impact of Greenland meltwater on deepwater formation in the North Atlantic Ocean. *Nature Geoscience*, *9*(7), 523–527. https://doi.org/10.1038/ngeo2740

Bullister, J. L. (2017). Atmospheric histories (1765-2015) for CFC-11, CFC-12, CFC-113, CCl4, SF6 and N2O. Oak Ridge, Tennessee: Carbon Dioxide Information Analysis Center. Oak Ridge National Laboratory, US Department of Energy.

Carter, B., Feely, R., Mecking, S., Cross, J., Macdonald, A., & Siedlecki, S. (2017). Two decades of pacific anthropogenic carbon storage and ocean acidification along global ocean ship-based hydrographic investigations program sections p16 and p02. *Global Biogeochemical Cycles*, *31*(2), 306–327.

DeGrandpre, M. D., Körtzinger, A., Send, U., Wallace, D. W. R., & Bellerby, R. G. J. (2006). Uptake and sequestration of atmospheric CO2 in the Labrador Sea deep convection region. *Geophysical Research Letters*, *33*(21), 1–5. https://doi.org/10.1029/2006GL026881

De Lavergne, C., Palter, J. B., Galbraith, E. D., Bernardello, R., & Marinov, I. (2014). Cessation of deep convection in the open Southern Ocean under anthropogenic climate change. *Nature Climate Change*, *4*(4), 278–282. https://doi.org/10.1038/nclimate2132

DeVries, T. (2014). The oceanic anthropogenic CO2 sink: Storage, air-sea fluxes, and transports over the industrial era. *Global Biogeochemical Cycles*, *28*(7), 631–647. https://doi.org/10.1002/2013gb004739

Dickson, A. G., & Millero, F. J. (1987). A comparison of the equilibrium constants for the dissociation of carbonic acid in seawater media. *Deep Sea Research Part A. Oceanographic Research Papers*, *34*(10), 1733–1743. https://doi.org/10.1016/0198-0149(87)90021-5

Dlugokencky, E., Mund, J., Crotwell, A., Crotwell, M., & Thoning, K. (2019). *Atmospheric carbon dioxide dry air mole fractions from the NOAA ESRL carbon cycle cooperative global air sampling network, 1968–2018 version: 2019-07*.

Environment & Climate Change Canada (2020). *National inventory report 1990–2018: Greenhouse gas sources and sinks in Canada*. Retrieved from www.canada.ca/en/environment-climate-change/services/climate-change/greenhouse-gas-emissions/inventory.html

Friis, K., Körtzinger, A., Pätsch, J., & Wallace, D. W. R. (2005). On the temporal increase of anthropogenic CO2 in the subpolar North Atlantic. *Deep Sea Research Part I: Oceanographic Research Papers*, *52*(5), 681–698. https://doi.org/10.1016/j.dsr.2004.11.017

Goodkin, N. F., Levine, N. M., Doney, S. C., & Wanninkhof, R. (2011). Impacts of temporal CO2 and climate trends on the detection of ocean anthropogenic CO_2 accumulation. *Global Biogeochemical Cycles*, *25*(3). https://doi.org/10.1029/2010gb004009

Gruber, N., Clement, D., Carter, B. R., Feely, R. A., Van Heuven, S., Hoppema, M., et al. (2019). The oceanic sink for anthropogenic CO2 from 1994 to 2007. *Science*, *363*(6432), 1193–1199. https://doi.org/10.1126/science.aau5153

Gruber, N., Landschützer, P., & Lovenduski, N. S. (2019). The variable Southern Ocean carbon sink. *Annual Review Of Marine Science*, *11*, 159–186. https://doi.org/10.1146/annurev-marine-121916-063407

Gruber, N., Sarmiento, J. L., & Stocker, T. F. (1996). An improved method for detecting anthropogenic CO2in the oceans. *Global Biogeochemical Cycles*, *10*(4), 809–837. https://doi.org/10.1029/96gb01608

Haine, T. W. N., & Richards, K. J. (1995). The influence of the seasonal mixed layer on oceanic uptake of CFCs. *Journal of Geophysical Research*, *100*(C6), 10727–10744. https://doi.org/10.1029/95jc00629

Hall, T., Haine, T., & Waugh, D. (2002). Inferring the concentration of anthropogenic carbon in the ocean from tracers. *Global Biogeochemical Cycles*, *16*(4). https://doi.org/10.1029/2001gb001835

Hall, T. M., Waugh, D. W., Haine, T. W., Robbins, P. E., & Khatiwala, S. (2004). Estimates of anthropogenic carbon in the Indian Ocean with allowance for mixing and time-varying air-sea CO2 disequilibrium. *Global Biogeochemical Cycles*, *18*(1). https://doi.org/10.1029/2003gb002120

Holzer, M., & Hall, T. M. (2000). Transit-time and tracer-age distributions in geophysical flows. *Journal of the Atmospheric Sciences*, *57*(21), 3539–3558. https://doi.org/10.1175/1520-0469(2000)057<3539:ttatad>2.0.co;2

Hsieh, P.-Y. (2016). *Deconvolution of the Labrador Sea transit-time distribution from combined measurements of CFC-11 and CFC-12 (Unpublished doctoral dissertation)*. UC Irvine.

Khatiwala, S., Primeau, F., & Hall, T. (2009). Reconstruction of the history of anthropogenic CO2 concentrations in the ocean. *Nature*, *462*(7271), 346–349. https://doi.org/10.1038/nature08526

Khatiwala, S., Tanhua, T., Mikaloff Fletcher, S., Gerber, M., Doney, S. C., Graven, H. D., et al. (2013). Global ocean storage of anthropogenic carbon. *Biogeosciences*, *10*(4), 2169–2191. https://doi.org/10.5194/bg-10-2169-2013

Koelling, J., Wallace, D. W. R., Send, U., & Karstensen, J. (2017). Intense oceanic uptake of oxygen during 2014–2015 winter convection in the Labrador Sea. *Geophysical Research Letters*, *44*(15), 7855–7864. https://doi.org/10.1002/2017gl073933

Körtzinger, A., Send, U., Wallace, D. W. R., Karstensen, J., & DeGrandpre, M. (2008). Seasonal cycle of O_2 and pCO_2 in the central Labrador Sea: Atmospheric, biological, and physical implications. *Global Biogeochemical Cycles*, *22*(1). https://doi.org/10.1029/2007gb003029

Lauvset, S. K., & Tanhua, T. (2015). A toolbox for secondary quality control on ocean chemistry and hydrographic data. *Limnology and Oceanography: Methods*, *13*(11), 601–608. https://doi.org/10.1002/lom3.10050

Lewis, E., Wallace, D., & Allison, L. (1998). *Program developed for CO2 system calculations*. Carbon Dioxide Information Analysis Center, managed by Lockheed Martin Energy Research Corporation for the US Department of Energy Tennessee. https://doi.org/10.2172/639712

Matsumoto, K., & Gruber, N. (2005). How accurate is the estimation of anthropogenic carbon in the ocean? An evaluation of the Δc* method. *Global Biogeochemical Cycles*, *19*(3). https://doi.org/10.1029/2004gb002397

Mehrbach, C., Culberson, C. H., Hawley, J. E., & Pytkowicx, R. M. (1973). Measurement of the apparent dissociation constants of carbonic acid in seawater at atmospheric pressure1. *Limnology & Oceanography*, *18*(6), 897–907. https://doi.org/10.4319/lo.1973.18.6.0897

Olsen, A., Key, R. M., van Heuven, S., Lauvset, S. K., Velo, A., Lin, X., et al. (2016). The global ocean data analysis project version 2 (GLODAPv2)—an internally consistent data product for the world ocean. *Earth System Science Data*, *8*(2), 297–323. https://doi.org/10.5194/essd-8-297-2016

Prinn, R. G., Weiss, R. F., Fraser, P. J., Simmonds, P. G., Cunnold, D. M., Alyea, F. N., et al. (2000). A history of chemically and radiatively important gases in air deduced from ale/gage/agage. *Journal of Geophysical Research*, *105*(D14), 17751–17792. https://doi.org/10.1029/2000jd900141

Punshon, S., Childs, D., & Azetsu-Scott, K. (2016). A purge-and-trap gas chromatographic method for shipboard determination of the transient tracers sulphur hexafluoride and dichlorodifluoromethane in seawater and in air. *Canadian Technical Report of Hydrography and Ocean Sciences*, *309*, 21.

Raimondi, L., Matthews, J. B. R., Atamanchuk, D., Azetsu-Scott, K., & Wallace, D. W. R. (2019). The internal consistency of the marine carbon dioxide system for high latitude shipboard and in situ monitoring. *Marine Chemistry*, *213*, 49–70. https://doi.org/10.1016/j.marchem.2019.03.001

Rhein, M., Steinfeldt, R., Kieke, D., Stendardo, I., & Yashayaev, I. (2017). Ventilation variability of labrador sea water and its impact on oxygen and anthropogenic carbon: a review. *Philosophical Transactions Of the Royal Society A*, *375*(2102), 20160321. https://doi.org/10.1098/rsta.2016.0321

Roemmich, D. (1983). Optimal estimation of hydrographic station data and derived fields. *Journal of Physical Oceanography*, *13*(8), 1544–1549. https://doi.org/10.1175/1520-0485(1983)013<1544:oeohsd>2.0.co;2

Sabine, C. L., Feely, R. A., Gruber, N., Key, R. M., Lee, K., Bullister, J. L., & Rios, A. F. (2004). The oceanic sink for anthropogenic CO2. *Science*, *305*(5682), 367–371. https://doi.org/10.1126/science.1097403

Sabine, C. L., & Tanhua, T. (2010). Estimation of anthropogenic CO2 inventories in the ocean. *Annual Review Of Marine Science*, *2*, 175–198. https://doi.org/10.1146/annurev-marine-120308-080947

Schneider, A., Tanhua, T., Körtzinger, A., & Wallace, D. W. (2010). High anthropogenic carbon content in the eastern Mediterranean. *Journal of Geophysical Research*, *115*(C12). https://doi.org/10.1029/2010jc006171

Sloyan, B. M., Wanninkhof, R., Kramp, M., Johnson, G. C., Talley, L., & Tanhua, T. (2019). The global ocean ship-base hydrographic investigations program (go-ship): A platform for integrated multidisciplinary ocean science. *Frontiers in Marine Science*, *6*, 445. https://doi.org/10.3389/fmars.2019.00445

Smethie, W. M., Jr, & Fine, R. A. (2001). Rates of North Atlantic deep water formation calculated from chlorofluorocarbon inventories. *Deep Sea Research Part I: Oceanographic Research Papers*, *48*(1), 189–215. https://doi.org/10.1016/s0967-0637(00)00048-0

Smith, J. N., Smethie, W. M., Yashayev, I., Curry, R., & Azetsu-Scott, K. (2016). Time series measurements of transient tracers and tracer-derived transport in the deep western boundary current between the Labrador Sea and the subtropical Atlantic Ocean at line w. *Journal of Geophysical Research: Oceans*, *121*(11), 8115–8138. https://doi.org/10.1002/2016jc011759

Steinfeldt, R., Rhein, M., Bullister, J. L., & Tanhua, T. (2009). Inventory changes in anthropogenic carbon from 1997–2003 in the Atlantic Ocean between 20°S and 65°N. *Global Biogeochemical Cycles*, *23*(3). https://doi.org/10.1029/2008gb003311

Stramma, L., Kieke, D., Rhein, M., Schott, F., Yashayaev, I., & Koltermann, K. P. (2004). Deep water changes at the western boundary of the subpolar North Atlantic during 1996 to 2001. *Deep Sea Research Part I: Oceanographic Research Papers*, *51*(8), 1033–1056. https://doi.org/10.1016/j.dsr.2004.04.001

Tait, V. K., Gershey, R. M., & Jones, E. P. (2000). Inorganic carbon in the Labrador Sea: Estimation of the anthropogenic component. *Deep Sea Research Part I: Oceanographic Research Papers*, *47*(2), 295–308. https://doi.org/10.1016/s0967-0637(99)00059-x

Takahashi, T., Feely, R. A., Weiss, R. F., Wanninkhof, R. H., Chipman, D. W., Sutherland, S. C., & Takahashi, T. T. (1997). Global air-sea flux of CO2: An estimate based on measurements of sea-air pCO2 difference. *Proceedings of the National Academy of Sciences*, *94*(16), 8292–8299. https://doi.org/10.1073/pnas.94.16.8292

Tanhua, T., & Keeling, R. F. (2012). Changes in column inventories of carbon and oxygen in the Atlantic Ocean. *Biogeosciences*, *9*, 4819–4833. https://doi.org/10.5194/bg-9-4819-2012

Tanhua, T., Waugh, D. W., & Wallace, D. W. (2008). Use of SF6 to estimate anthropogenic CO2 in the upper ocean. *Journal of Geophysical Research: Oceans*, *113*(C4). https://doi.org/10.1029/2007jc004416

Terenzi, F., Hall, T., Khatiwala, S., Rodehacke, C., & LeBel, D. (2007). Uptake of natural and anthropogenic carbon by the Labrador Sea. *Geophysical Research Letters*, *34*(6). https://doi.org/10.1029/2006gl028543

Van Heuven, S., Pierrot, D., Rae, J., Lewis, E., & Wallace, D. (2011). MATLAB Program Developed for CO2 System Calculations. In RNL/CDIAC-105b. Carbon Dioxide Information Analysis Center. Oak Ridge, TN: Oak Ridge National Laboratory, US Department of Energy. https://doi.org/10.3334/cdiac/otg.co2sys_matlab_v1.1

van Heuven, S. M., Hoppema, M., Huhn, O., Slagter, H. A., & de Baar, H. J. (2011). Direct observation of increasing co2 in the weddell gyre along the prime meridian during 1973–2008. *Deep Sea Research Part II: Topical Studies in Oceanography*, *58*(25–26), 2613–2635. https://doi.org/10.1016/j.dsr2.2011.08.007

Walker, S. J., Weiss, R. F., & Salameh, P. K. (2000). Reconstructed histories of the annual mean atmospheric mole fractions for the halocarbons CFC-11, CFC-12, CFC-113, and carbon tetrachloride. *Journal of Geophysical Research*, *105*(C6), 14285–14296. https://doi.org/10.1029/1999jc900273

Wallace, D. (2001). Introduction to special section: Ocean measurements and models of carbon sources and sinks. *Global Biogeochemical Cycles*, *15*(1), 3–10. https://doi.org/10.1029/2000gb001354

Wallace, D. W. (1995). Monitoring global ocean carbon inventories. *Ocean Observing System Development Panel*.

Wallace, D. W., & Lazier, J. R. N. (1988). Anthropogenic chlorofluoromethanes in newly formed Labrador Sea water. *Nature*, *332*(6159), 61–63. https://doi.org/10.1038/332061a0

Waugh, D. W., Hall, T. M., McNeil, B. I., Key, R., & Matear, R. J. (2006). Anthropogenic CO2 in the oceans estimated using transit time distributions. *Tellus B: Chemical and Physical Meteorology*, *58*(5), 376–389. https://doi.org/10.1111/j.1600-0889.2006.00222.x

Yashayaev, I. (2007). Hydrographic changes in the Labrador Sea, 1960-2005. *Progress in Oceanography*, *73*(3–4), 242–276. https://doi.org/10.1016/j.pocean.2007.04.015

Yashayaev, I., & Dickson, B. (2008). Transformation and fate of overflows in the northern North Atlantic. In Arctic–subarctic ocean fluxes (pp. 505–526). Springer. https://doi.org/10.1007/978-1-4020-6774-7_22

Yashayaev, I., & Loder, J. W. (2016). Recurrent replenishment of Labrador Sea Water and associated decadal-scale variability. *Journal Of Geophysical Research: Oceans*, *121*(11), 8095–8114. https://doi.org/10.1002/2016jc012046

Yashayaev, I., & Loder, J. W. (2017). Further intensification of deep convection in the Labrador Sea in 2016. *Geophysical Research Letters*, *44*(3), 1429–1438. https://doi.org/10.1002/2016gl071668